Journal of Materials Chemistry A

Accepted Manuscript

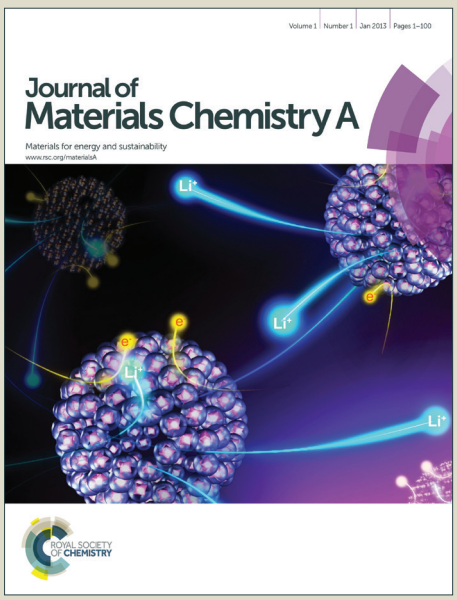

ROYAL SOCIETY OF CHEMISTRY

www.rsc.org/materialsA

Theoretical insight into highly durable iron phthalocyanine derived non-precious catalyst for oxygen reduction reaction

Min Ho Seo[a], Drew Higgins[a], Gaopeng Jiang[a], Sung Mook Choi[b], Byungchan Han[c]* and Zhongwei Chen[a]*

[a] *Department of Chemical Engineering, Waterloo Institute for Nanotechnology, Waterloo Institute of Sustainable Energy, University of Waterloo, 200 University Ave. W, Waterloo, ON, N2L 3G1, Canada,* [b] *Surface Technology Division, Korea Institute of Materials Science (KIMS), Changwon 641-010, South Korea.* [c]*Department of Energy Systems Engineering, Daegu Gyeongbuk Institute of Science and Technology (DGIST), Daegu, 711-873, South Korea, School of Materials Science and Engineering,*

* Corresponding author

E-mail address: zhwchen@uwaterloo.ca[a], hanbc@dgist.ac.kr[c],

Tel: +1-519-888-4567 ext. 38664 [a], +82-53-785-6412[c]

Fax: +1-519-746-4347 [a], +82-53-785-6409 [c]

Abstract

N_4-chelate macrocycles comprise the foundation for non-precious metal oxygen reduction reaction (ORR) catalyst research, the main electrochemical process occurring in polymer electrolyte membrane (PEM) fuel cells. Although iron-nitrogen-carbon (M-N-C) complexes are known as the most active non-precious ORR catalysts to date, fundamental understanding of the ORR mechanisms on these materials is still immature and further investigations are needed. In this work, ab-initio density functional theory (DFT) calculations are applied to unveil the underlying principles for electrocatalytic activity and structural stability of Fe-N4 chelates exposed to acidic media. To accomplish this, we compare the electronic structures of ferrous phthalocyanine (Fe-Pc) and an in-house developed Fe-Pc modified with diphenylphenthioether substituent species (Fe-SPc). The results of these DFT simulations are directly correlated with results of half-cell ORR activity and stability electrochemical testing in 0.1 M $HClO_4$. The results indicate that the relative energetic position of the d_{z2}-orbital with respect to the Fermi level can induce a Fe redox couple potential shift and modulate the catalytic activity towards the ORR. Furthermore, our combined DFT calculations and empirical observations highlight that the relative position of the d_{z2}-orbital can be controlled by the incorporation of functional groups, resulting in the ability to tune the ORR activity of these complexes. Structural stability of the materials is also predicted by the DFT calculated cohesive energies of Fe and FeO, which can also be readily tuned by modulating Fe-Pc with substituent species. This study, coupling rigorous experimental observations with DFT investigations thereby provides fundamental insight that can aid in the design of future generation of non-precious ORR catalysts with improved activity and stability.

Keywords: metal-N4 chelates macrocycle catalyst, oxygen reduction reaction , nonprecious catalyst, density functional theory, polymer electrolyte membrane fuel cell

1. Introduction

Accurate understanding of oxygen reduction reaction (ORR) mechanisms is vital for improving the efficiency of many devices, including metal-air batteries[1-5], fuel generation devices[6, 7] and fuel cells[8-14]. This issue is highly pertinent in proton exchange membrane (PEM) fuel cells, which are non-polluting electrochemical power generation devices that convert chemical energy of fuels into electricity, heat and water. Despite the clean and thermodynamically efficient operation of these devices, there are many technical and economic challenges which still prevent their widespread application[9-11, 15-17]. The main obstacles are the inherently sluggish ORR kinetics and the low durability of catalysts under the harsh operating conditions[18-20]. Until now, the best and most widely used catalysts are expensive Pt-based materials, owing to their relatively high activity and stability in acidic media[19-22] in comparison to other metal and non-metal based catalysts. The reliance on high-priced Pt catalysts has provided economical motivation to develop various non-precious ORR catalyst materials, including transition metal-N_4 chelate macrocycles, nitrogen-doped carbons, and metal-nitrides, oxides and chalcogenides[23-27].

Transition metal-nitrogen-carbon (M-N-C) complexes based on iron, first prepared by heat treatment of Fe-N_4 chelate macrocycles, or more recently, relatively inexpensive inorganic and organic precursors[26-32], have emerged as the most promising non-precious catalysts. It has been well established that a heat treatment at temperatures ranging from ca. 700 to 1000 ^{o}C is important for imparting high catalyst activity and stability. Significant structural reconfiguration and the heterogeneous complexity of the M-N-C materials resulting from the heat treatment have however led the majority of studies to rely on trial and error based approaches. These investigations involve empirical optimization of various thermodynamic and kinetic variables

by systematically varying the catalyst synthesis procedures (i.e. precursor types and concentrations, mixing/blending strategies, heat-treatment temperatures and treatment durations, post-treatment procedures, etc.). In addition, vague understanding of the active sites in M-N-C catalysts has further made the fundamental elucidation of the mechanisms underlying ORR activity and stability an immense challenge. Without this knowledge, it is impossible to apply rational design strategies to prepare non-precious ORR catalysts with improved activity and stability in PEM fuel cells.

Previously, we reported a new iron phthalocyanine (Fe-Pc) based material functionalized with four diphenylphenthioether substituent species (Fe-SPc) as a non-precious ORR catalyst and investigated the half-cell electrochemical properties in 0.1 M $HClO_4$[33]. Fe-SPc was prepared *in lieu* of a pyrolysis process, enabling the ability to adequately control the atomic structure and surface properties of the Fe-SPc materials. Significantly improved electrochemical stability of Fe-SPc was observed in comparison to Fe-Pc catalyst, attributed to the incorporation of thioether substituent groups that were *speculated* to provide electron donating capabilities to the metal-ion center. Conclusively explaining the electrochemical performance variations between Fe-Pc and Fe-SPc and understanding the electronic structure-property relationships of this class of materials will provide valuable fundamental insight that can guide future catalyst design endeavors.

To fundamentally elucidate the structural properties and explain empirical results with fundamental catalytic mechanistic understanding for a variety of different materials and reactions, *ab-initio* computational methods using density functional theory (DFT) has emerged as a very useful tool[34-37]. For example, *ab-initio* computational studies have been used to confirm Sabatier's principle, whereby a good electrocatalyst should have moderate chemical

interactions with reaction intermediates[34-37]. This led to the proposition that a simple electronic structure parameter, the d-band center, could successfully dictate the ORR kinetics occurring on a wide array of materials[38-41]. According to this principle, N4-chelate macrocycles should also provide finite chemisorption energies between the oxygen intermediates and ORR active surface sites, and a certain value exists that can maximize ORR turnover frequencies.

It is known that the electronic structure of a metal ion can be modified by the surrounding π-conjugated ligand topologies, thereby causing a change of its redox potential[34, 42, 43]. This implies that variations in the electronic properties of the overall macrocycle structures are governed by contributions from both the metal-ion center and the surrounding ligand structure. As such, it is necessary to prepare well-defined model systems and develop accurate molecular orbital analysis to acquire a fundamental understanding of ORR catalytic activity. In the present work, we utilize first principles DFT calculations to understand particular mechanisms governing the catalytic activity and structural stability of Fe-SPc and Fe-Pc materials from the perspective of macrocycle electronic structure. Empirical electrochemical measurements published previously[33] were used in combination with molecular orbital analysis to identify the key fundamental factors controlling ORR activity and long-term stability, most importantly the electron transfer mechanisms occurring at the molecular scale.

2. Computational design and Experimental procedures

Computational Details

Density functional theory (DFT) [44, 45] calculations implemented in Vienna ab initio simulation package (VASP) [46] program were utilized for the present study. Exchange-

correlation energies of electrons are described by the Perdew, Burke and Ernzerhof (PBE) functional[47] for generalized gradient approximation (GGA)[48]. Core electrons were replaced by the projector augmented wave (PAW) pseudo-potentials[49, 50], and Kohn-Sham wave functions of valence electrons were expanded by plane wave basis set with a cutoff energy of 520 eV. The designed Fe-Pc and Fe-SPc are located at the center of vacuum cube box having lengths of 40 Å for all x, y and z direction. The atoms and cell parameters of each structure were fully relaxed and spin polarized calculations were performed. A Gamma point mesh of 1 × 1 × 1 was used for the calculation of density of states (DOS) and for finding thermodynamically stable Fe-SPc and Fe-Pc structures with a Gaussian-smearing width of 0.2 eV[51, 52].

Synthesis of ferrous 2,9,16,23-tetra(2',6'-diphenylphenthio ether) phthalocyanine (Fe-SPc)

Fe-SPc was prepared according to the method reported in our previous study[33]. In brief, and depicted schematically in Fig. 1., 4-nitrophthalonitrile and Fe(OAc)2 were dissolved in 100 ml of quinolone and stirred at 483 K under N_2 protection. After 24 hours, methanol was added to precipitate the materials, and a green powder consisting of ferrous 2,9,16,23-tetranitro phthalocyanine (Fe-(nitro)Pc) was obtained by purification with column chromatography on a silica gel with pyridine as the eluent. The 2, 6-diphenylthiophenol, Cs_2CO_3, N-Methylpyrrolidone (NMP), and toluene were stirred at 418 K under N_2 atmosphere until the water and toluene evaporated, after which the mixture was cooled. Prepared Fe-(nitro)Pc was then added into the reaction mixture under N_2 protection and heated at 453 K while stirring for 12 h. After cooling, the mixture was poured into methanol to precipitate the resulting green powder which was purified by column chromatography on silica gel with dichloromethane.

Electrode preparation and electrochemical measurements

The electrode preparation and electrochemical analysis carried out previously are summarized in this section[33]. Electrochemical measurements were performed via cyclic voltammetry (CV) using a bipotentiostat (PINE research instrumentation). The half-cell system consisted of a pre-treated glassy carbon working electrode (0.196 cm^2), platinum wire counter electrode and reference electrode (Reversible Hydrogen Electrode, Hydroflex™, RHE). The Fe-SPc is refluxed for 2 h on KJ300 which is sonicated in 1,2-dichloroethane then the Fe-SPc/KJ300 was collected after the solvent was distilled off. 20 mg of Fe-SPc was dissolved in 5 mL of 1,2-dichloroethane at the same time. Catalyst inks were prepared as follows: 2 mg catalyst samples were suspended in 1 mL of ethanol and a Nafion® ionomer solution (5 wt.%) and sonicated then pipetted 60 uL of catalyst solution was transferred to working electrode. N_2 or O_2 gas was purged into the electrolyte for at least 30 min before performing electrochemical measurements. The ORR polarization curves for the RDE were obtained in an O_2-saturated 0.1 M $HClO_4$ solution at room temperature. A positive sweep was performed at a scan rate of 10 mV s^{-1} and electrode rotation rates of 400, 900, 1600 and 2500 rpm.

3. Results and discussion

To understand the mechanistic origin of ORR activity and structural stability of Fe-SPc in acidic conditions, four possible positional isomers (e.g., Cs, C2v, D2h and C4h symmetry) were designed by replacing H atoms on each of the four external heterocycles in Fe-Pc with diphenylthiophenol substituent groups. The C4h structure showed the most stable structure which is consistent with our previous reports[33]. Fig. 2a and 2b shows the DFT optimized Fe-Pc

and Fe-SPc structures, respectively. The structure of Fe-Pc was optimized as a nearly planar macrocycle structure, whereas the Fe-SPc appears to undergo structural distortion owing to the diphenyl thiophenol groups. The bond lengths between the central Fe atom and surrounding N atoms denoted as N1, N2, N3 and N4 in Fig. 2 were calculated to be ca. 1.93 - 1.94 Å in Fe-Pc as summarized in Table 1 and consistent with previous reports[53]. It has been proposed that the changes in the molecular geometry, particularly the Fe-N bonding lengths, arise due to the modulated electronic properties of the metal-center, induced by the effect the diphenyl thiophenol groups have on the surrounding ligand structures in Fe-SPc.[24,33,44,45] We verified this speculation by calculating the atomic partial charges on Fe-Pc and Fe-SPc and related the structural change to the nature of the Fe metal-center. We believe that the central Fe-ion may have significant orbital hybridizations with the surrounding N atoms and affect catalytic performance. Figures 3a and 3b display the differences in the charge density, which are defined by equation (1),

$$\rho = \rho_{Fe-(S)Pc} - \rho_C - \rho_N - \rho_H - \rho_{Fe}(-\rho_S) \quad (1)$$

The yellow and blue areas in Fig. 3 indicate the electronic charge accumulation and depletion, respectively. Both Fe-Pc and Fe-SPc show that the electronic charge distribution is symmetric, and that the charges are accumulated around the nitrogen (N) atoms owing to its high electronegativity (3.04) on the Pauling scale[54]. The central Fe-ion in Fe-Pc demonstrates a depletion of charge, whereas the addition of electron-donating diphenyl thiophenol functional groups on Fe-SPc leads to a charge accumulation . The projected density of states (PDOS) of the valence Fe electrons are provided in Fig. 4, demonstrating that the electronic structure of Fe-SPc changes significantly with respect to Fe-Pc. The DOS of Fe in Fe-Pc and Fe-SPc displayed in Fig. 4a and 4b, respectively, demonstrate bonding-antibonding splitting, which

provides indication of the strong chemical bonds between the metal and non-metal atoms.[38, 55, 56]. The octahedral environment gives rise to doubly and triply degenerated e_g and t_{2g} sets which consist of the axial orbitals of d_{x2-y2} and d_{z2}, and the interaxial of d_{xy}, d_{xz}, and d_{yz} orbitals[34, 43, 57, 58]. Figure 4 demonstrates occupied and unoccupied molecular orbitals for the ground states of the Fe-Pc and Fe-SPc molecules. For Fe-Pc and Fe-SPc with local octahedral symmetry (or square planar symmetry, C_{4h}) coordination of the Fe center, the uppermost band is built of d_{x2-y2} levels, an observation consistent with previous reports[34, 43, 57-59]. In the PDOS for the 3d electrons of Fe in Fe-Pc (Fig. 4a), the electrons of Fe-t_{2g} like bands (e.g., d_{xy}, d_{xz}, and d_{yz}) in the up-spin state are almost fully occupied, whereas those in a down-spin state are half filled near the Fermi level. In contrast, adding a diphenyl thiophenol functional group on Fe-Pc shifts the Fermi energy to a more positive value, and the electronic t_{2g} like orbital near the Fermi level is fully filled for Fe-SPc, attributed to the additional electrons provided by the ring ligands as demonstrated in Fig. 3.

To understand ORR activity mechanism from molecular orbital analysis, we designed model systems including either O_2 or O adsorbed on Fe-Pc and Fe-SPc as shown in Fig. 5. From the optimized structures, the bonding lengths between Fe and the nearest neighbored O atom of O_2, which are directly associated with adsorption energy of O_2 on Fe in macrocycle complexes, were evaluated to be 1.813 Å and 1.812 Å for Fe-Pc and Fe-SPc, respectively. Figure 6a and 6b illustrate that the d_{x2-y2} orbital in the projected-density of states (PDOS) does not directly link with O_2 adsorption on both Fe-Pc and Fe-SPc, showing that the peaks for the d_{x2-y2} orbital are in fact formed without the effect of split-off bands and indicating strong chemisorption. However, Figure 6c and 6d show that the electronic d_{z2} orbital is spilt into bonding and antibonding states before and after the adsorption of O_2, meaning that the d_{z2} orbital in the PDOS is more of a

dominant factor influencing ORR activity. This in turn highlights that the d_{z2} orbital is closely linked with the redox potential of the Fe-ion, a value that has been well established to govern the onset potential for ORR on these macrocycle materials[34, 60-62,]. The triangles in Fig. 6c and 6d demonstrate that the level of the d_{z2} orbitals in the up-spin state and under the Fermi level in Fe-SPc is shifted upward in comparison to the Fe-Pc from -2.158 eV to -2.085 eV.

To truly identify the relationship between the d_{z2} orbital and the ORR activity, the Fe-SPc and Fe-Pc supported on KJ300 were subjected to rotating disk electrode (RDE) voltammetry as shown in our previous work[33]. The ORR is a multi-electron transfer reaction with two primary pathways[63-65]. The first is the transfer of two electrons to produce hydrogen peroxide[63-65], H_2O_2, and the second is the direct four-electron pathway to produce water, H_2O, described as the following reaction (2, 3)[63, 65].:

$$O_2 + 2H_2 + 2e^- \rightarrow H_2O_2 \tag{2}$$

$$O_2 + 4H^+ + 4e^- \rightarrow 2H_2O \tag{3}$$

The ORR polarization curves of the catalysts were obtained at rotation rates varying from 400 to 2500 rpm in O_2-saturated 0.1 M $HClO_4$ electrolyte. After removing background currents to eliminate capacitive contributions, the number of electrons transferred for the reduction of O_2 on both Fe-Pc and Fe-SPc was calculated to be ca. 4 by the Koutecky-Levich equation (4)[66, 67]:

$$\mathrm{i_d} = 0.62\mathrm{n_e FSD}_{O_2}^{2/3}\nu^{-1/6}\mathrm{c}_0\omega^{1/2} = \mathrm{B}\omega^{1/2} \tag{4}$$

Here, i_d is the disk current density, n_e is the number of electrons transferred per molecule of O_2, F is Faraday's constant, S is geometric surface area of electrode, D_{O2} is the diffusion coefficient of dissolved O_2 in the electrolyte, ν is the kinematic viscosity of the electrolyte, ω is the electrode rotation rate in radian s^{-1}, c_0 is the concentration of dissolved O_2 in electrolyte and B is the Levich constant. In Fig. 7a as previously reported[33], the polarization curves

obtained in O_2 saturated 0.1 M $HClO_4$ at 298 K using a potential scan rate of 10 mV s^{-1} from 0 to 1.0 V vs. RHE and at the rotation speed of 400 rpm are provided. Here, Fe-Pc/KJ300 demonstrates an increased on-set potential and a half-wave potential (0.62 V vs. RHE) that is 20 mV higher than that of Fe-SPc/KJ300 (0.60 V vs. RHE), indicating better ORR performance without the addition of the diphenyl thiophenol substituent groups.

The first electron transfer to adsorbed O_2 to form superoxide species is generally considered the factor that governs the onset potential for ORR[61, 68, 69]. The mechanism can be expressed by equation (5) and (6):

$$O_2 \rightarrow O_2^* \tag{5}$$

$$O_2^* + e^- \rightarrow O_2^- \tag{6}$$

Here, O_2^* is the adsorption of O_2 on catalyst surface. The energy difference (ΔO2p) between the Fermi level and peak positions of the unoccupied O2p orbital, denoted as an asterisk in the PDOS for adsorbed O_2 (Fig. 7b and 7c) could provide insight into the first electron transfer reaction (5), whereby smaller ΔO2p values indicate an easier electron transfer. The energy level of the O2p orbital in the antibonding states of O_2 with down spin states are 0.477 eV and 0.481 eV for Fe-Pc and Fe-SPc, respectively. Therefore, the higher onset potential of Fe-Pc in Fig. 7a could be interpreted from the computational results which indicate that the ΔO2p value of Fe-Pc is smaller than that of Fe-SPc, leading to a relatively easier electron transfer to the O atom, and therefore improved ORR kinetics. From these observations, it can be inferred that the lower ORR onset potential of Fe-SPc is attributed to the electronic structure changes of the central Fe atom induced by adding the electronic donating substituents that result in an upward shift of the e_g (d_{z2}) orbital and limits the electron transferability to adsorbed O_2 molecules.

Using the calculated thermodynamics of different intermediates, we make direct comparisons

to voltammetric and rotating ring disk electrode experiments to evaluate the electrochemical activity of the Fe-Pc and Fe-SPc surface for ORR. With the DOS studies, thermodynamic free energy diagrams were calculated to define a rate determine step of the ORR on Fe-Pc and Fe-SPc surfaces. Four electron reaction paths were considered as shown in equations (6)-(9):

$$O_2(g) + 4H^+ + 4e^- \rightarrow OOH^* + 3H^+ + 3e^- \quad (6)$$

$$OOH^* + 3H^+ + 3e^- \rightarrow O^* + H_2O(l) + 2H^+ + 2e^- \quad (7)$$

$$O^* + H_2O(l) + 2H^+ + 2e^- \rightarrow [OH]^* + H_2O(l) + H^+ + e^- \quad (8)$$

$$[OH]^* + H_2O(l) + H^+ + e^- \rightarrow 2H_2O \quad (9)$$

The details regarding ORR free energy diagram calculations are well described in previous published reports[70-73]. Briefly, the free energy of any ORR intermediate with respect to liquid H_2O (ΔG) was calculated using equation (10):

$$\Delta G = \Delta E + \Delta ZPE - T\Delta S \quad (10)$$

Here, ΔE, ΔZPE and ΔS denote the DFT calculated ground state energy, zero point energy, and entropy corrections, respectively. The ΔZPE for intermediates were adopted from Nørskov *et al.*[70], which used ΔS at T= 298 K as presented by a thermodynamic table[70, 74]. The effect of the potential was evaluated at pH=0 by shifting the electronic chemical potential according to Nernst's law. Figure 8 demonstrates the free energy change of each ORR step for ideal, Fe-Pc and Fe-SPc at zero electrode potential (Φ = 0V vs. RHE) and at the potential for which all steps become energetically negative. At the equilibrium potential (U = 1.23V), the O^* formation is energetically negative (exothermic) and all other step are positive (endothermic) on both of Fe-Pc and Fe-SPc. By applying overpotential, all steps become negative for the ORR at 0.67 V and 0.59 V vs. RHE on the Fe-Pc and Fe-SPc, respectively. The calculated thermodynamic free energy diagram predicts that Fe-SPc activity is lower than that of Fe-Pc, consistent with RDE

experimental results. With even a slightly lower overpotential than the potential at which every reaction step is energetically negative (i.e., 0.67 and 0.59 V vs. RHE for Fe-Pc and Fe-SPc), the reduction step of O* to OH* will become energetically positive, revealing that the O*/OH* exchange is rate-determining for the ORR.

To investigate the impact of adsorption strength on ORR activity, the adsorption energy (E_{adss}) of the O or O_2 molecules on these macrocycle complexes are calculated by equation (11):

$$E_{ads} = E_{O_{(2)}Fe-(S)Pc} - E_{Fe-(S)Pc} - E_{O_{(2)},g} \tag{11}$$

Here, $E_{O_{(2)}Fe-(S)Pc}$, is the total energy of O or O_2 adsorbed Fe-Pc and Fe-SPc, $E_{Fe-(S)Pc}$ is the total energy of Fe-Pc and Fe-SPc, and $E_{O_{(2)},g}$ is total energy of O_2 (or O) in a vacuum. The DFT O_2 and O adsorption energies of Fe-SPc are evaluated to be -0.98 eV and -4.37 eV, respectively, which are higher than -0.92 eV and -4.02 eV of Fe-Pc. Fe-O bonding lengths of 1.644 Å and 1.642 Å and Fe-O_2 bonding lengths of 1.813 Å and 1.812 Å were determined for Fe-Pc and Fe-SPc, respectively. These results demonstrate that larger adsorption energies could result in shorter bonding distances. Therefore, the relatively upward shift of the d_{z2} orbital of Fe atoms provides stronger bonding of oxygen intermediates on Fe-SPc as indicated by our computational analysis. It can be interpreted that this enhanced adsorption strength with oxygen intermediates on Fe-SPc is too strong to obtain high activity for the ORR. Accordingly, a downshift in the energy level of the d_{z2} orbital away from the Fermi level leads to a shift in the Fe ion's redox potential, and by extension smaller ΔO2p values and higher ORR activity potentials. In summary, the ORR activity of metal macrocycle complexes is governed by the relative position of the d_{z2} orbital of Fe in comparison to the Fermi level, leading to the peak positions of the unoccupied O2p orbital in comparison to the Fermi level. Optimized adsorption strengths of the ORR intermediates could be achieved by control of the d_{z2} orbital level, which

could be downshifted by the attachment of electron withdrawing functional groups.

It has been proposed that the main degradation mechanism of Fe-N_4 chelate macrocycle catalysts in acidic electrolytes is the demetalation of the macrocycles[43,49]. This leads to a dramatic loss in ORR performance because the resulting H_2Pc materials have very limited activity[53, 61]. The demetalation process is highlighted in reaction (12):

$$Fe-(S)Pc+2H^{+}=H_2(S)Pc+Fe^{+2} \tag{12}$$

The redox couples of Fe-Pc and Fe-SPc observed in the cyclic voltammograms (CV) of Fig. 9a and b indicate the presence of the Fe-ion centers in the macrocycle complexes. Diminishing charges of the redox couple can therefore provide evidence of the Fe-N4 demetalation[33, 60, 61]. Fig. 9 clearly demonstrates that functionalized diphenyl thiophenol groups on the Fe-Pc dramatically enhance the stability of Fe-SPc over 100 cycles in oxygen saturated electrolyte. After 100 cycles, the CV curve of Fe-Pc exhibits a significant loss in the redox charge transfer of Fe in comparison to the initial plot (Fig. 9a). This observation is in agreement with the significant loss of ORR activity (Fig. 9b), indicating the occurrence of Fe-Pc demetalation under these conditions. On the other hand, after 100 cycles Fe-SPc still maintains the distinct Fe-ion redox peaks (Fig. 9c), and shows only a 20.3 mV loss in half-wave potential for the ORR (Fig. 9d).

This pronounced increase in the electrochemical stability of the Fe-SPc macrocycle is of high interest, and was investigated by calculating the cohesive energies (E_{coh}) of Fe and FeO in ferrous phthalocyanine macrocycle complexes through the first principle calculations using equations (13) and (14):

$$E_{coh}=-(E_{Fe-(S)Pc}-E_{(S)Pc}-E_{Fe,g}) \tag{13}$$

$$E_{coh}=-(E_{FeO-(S)Pc}-E_{(S)Pc}-E_{FeO,g}) \tag{14}$$

Here, $E_{FeO-(S)Pc}$ is the total energy of O adsorbed on Fe-Pc and Fe-SPc, $E_{Fe,g}$ and $E_{FeO,g}$ are total energy of Fe and FeO in the gas phase, and $E_{(S)Pc}$ is total energy of the phthalocyanine macrocycle frame of Fe-Pc and Fe-SPc without central Fe atom. In the case of metals, it has proposed that the cohesive energy and electrochemical dissolution potential of the metal are strongly correlated[22, 72, 75-78], and a higher cohesive energy of the metal indicates a higher dissolution potential. Thus, the cohesive energies of Fe or FeO in the macrocycle complexes are likely related to the durability of iron based materials under harsh condition. DFT predicts, however, that the cohesive energy of Fe in the macrocycle complex is 9.80 eV for Fe-Pc, which is higher than 9.53 eV for Fe-SPc. These results do not align with our electrochemical measurements in acidic electrolytes discussed previously. Therefore, to provide reasonable explanation surrounding the observed demetalation of the ferrous phthalocyanine complex, the presence of oxygen requires consideration. In fact, it was found that the demetalation and activity losses of Fe-Pc and Fe-SPc were minimized under inert atmospheres, whereas the activity was significantly compromised in the presence of oxygen that would attack the active site structures[33, 53]. When oxygen is adsorbed on Fe-Pc and Fe-SPc, electron transfer from the central metal to the oxygen molecule could decrease the atomic radius of the central Fe, and thus the distance of the Fe-N bonds could be increased[33, 53]. Even in this work, the distance between the central Fe and N atoms is increased from ca. 1.93 Å to 1.96 Å for FePc and Fe-SPc upon the adsorption of oxygen, and these results agree well with previous investigations[53, 79]. The FeO cohesive energy of of 10.22 eV for Fe-SPc is higher than 10.15 eV for Fe-Pc as summarized Table. 1, indicating that the electrochemical stability in the presence of oxygen for Fe-SPc is enhanced in comparison to Fe-Pc. Therefore, the diphenyl thiophenol electron donating groups substituted onto the phthalocyanine complex could exclusively help to

suppress the demetalation and enhance the stability of Fe-SPc in the presence of oxygen which is the necessary reactant at the cathode of PEMFCs.

Conclusion

Using first-principles DFT calculations, we have studied the scientifically relevant ORR processes occurring on Fe-Pc and Fe-SPc materials in terms of electrochemical activity and stability. The results indicate that the d_{z2} orbital in the DOS is closely related with ORR activity, showing electronic d_{z2} orbital splitting into bonding and antibonding states before and after the adsorption of O_2. The position of the d_{z2} orbital of Fe in comparison to the Fermi level, a factor related to the unoccupied ΔO2p orbital level, ultimately determines the ORR onset potential and oxygen intermediate adsorption strengths of metal macrocycle complexes, owing to the modulated electron transfer capabilities to the O atom. The free energy diagram clearly indicates that a rate determining step is in the reduction step of O* to OH*, which means that the overall ORR kinetics are governed by the oxygen adsorption strength on Fe-Pc and Fe-SPc. The relatively upward shift of the d_{z2} orbital of the Fe atom in Fe-SPc provides stronger bonding of oxygen intermediates, leading to a reduction in activity towards the ORR. This prediction is consistent with results from electrochemical testing carried out in O_2 saturated acidic condition, whereby the on-set potential and a half-wave potential of Fe-SPc/KJ300 was reduced in comparison to Fe-Pc/KJ300. The free energy diagram prepared using DFT also predicts the same activity trends, whereby the activity of Fe-SPc is slightly lower than that of Fe-Pc. It is therefore clear that optimized adsorption strengths of ORR intermediates can be achieved by carefully tuning the level of the d_{z2} orbital. Interestingly, the electrochemical stability of Fe-SPc evaluated by accelerated testing protocols was significantly enhanced in the

presence of oxygen in comparison to Fe-Pc. From theoretical calculations, this observation is explained due to the increased cohesive energy of FeO for Fe-SPc in comparison to Fe-Pc. Furthermore, the diphenyl thiophenol electron donating groups substituted onto the phthalocyanine complex could help to suppress the demetalation of the macrocycle structure by providing extra electrons to the metal ion center. As these investigated electronic properties can be directly modulated by the appropriate selection and attachment of various substituent groups on the transition metal macrocycles, this comprehensive DFT study linked to experimental observations can provide the fundamental basis for the design of future generation non-precious ORR catalysts with improved activity and stability.

Acknowledgement

The authors specially thank Mr. Hey Woong Park at the University of Waterloo for discussion and comments. Financial support was provided by the DOE-EERE Fuel Cell Technologies Program (Project ID: FC107) for non-precious metal catalysis research led by the Los Alamos National Laboratory and the Catalysis Research for Polymer Electrolyte Fuel Cells (CaRPE FC) Network administered from Simon Fraser University and supported by Automotive Partnership Canada (APC) Grant No. APCPJ 417858 - 11 through the Natural Sciences and Engineering Research Council of Canada (NSERC). This research was also enabled by the use of computing resources provided by WestGrid and Compute/Calcul Canada and Korea Institute of Science and Technology Information (KISTI, KSC-2013-C2-008 and KSC-2013-C2-054) and by supported from the Global Frontier R&D Program (2013-073298) on Center for Hybrid Interface Materials (HIM), funded by the Ministry of Science, ICT & Future Planning. The New and Renewable Energy R&D Program (20113020030020) and the Leading Foreign Research Institute Recruitment Program through the National Research Foundation of Korea (NRF) under the Ministry of Knowledge Economy, Republic of Korea partly supported this research work.

References

1. H. W. Park, D. U. Lee, L. F. Nazar and Z. W. Chen, *J. Electrochem. Soc.*, 2013, 160, A344-A350.
2. D. U. Lee, H. W. Park, D. Higgins, L. Nazar and Z. W. Chen, *J. Electrochem. Soc*, 2013, 160, F910-F915.
3. H. Zhang, X. Zhong, J. C. Shaw, L. X. Liu, Y. Huang and X. F. Duan, *Energy Environ. Sci.*, 2013, 6, 2621-2625.
4. J. L. Shui, J. S. Okasinski, P. Kenesei, H. A. Dobbs, D. Zhao, J. D. Almer and D. J. Liu, *Nat. Commun.*, 2013, 4.
5. D. Higgins, Z. Chen, D. U. Lee and Z. Chen, *J. Mater. Chem. A*, 2013, 1, 2639-2645.
6. N. Lopez, D. J. Graham, R. McGuire, G. E. Alliger, Y. Shao-Horn, C. C. Cummins and D. G. Nocera, *Science*, 2012, 335, 450-453.
7. M. W. Kanan and D. G. Nocera, *Science*, 2008, 321, 1072-1075.
8. W. Vielstich, A. Lamm and H. A. Gasteiger, *Handbook of Fuel Cells Fundamentals Technology and Applications*, John Wiley & Sons Ltd., London, 2003.
9. F. Bidault, D. J. L. Brett, P. H. Middleton and N. P. Brandon, *J. Power Sources*, 2009, 187 39–48.
10. J. S. Park, S. H. Park, S. D. Yim, Y. G. Yoon, W. Y. Lee and C. S. Kim, *J. Power Sources* 2008, 178 620–626.
11. K. Asazawa, K. Yamada, H. Tanaka, A. Oka, M. Taniguchi and T. Kobayashi, *Angew. Chem.*, 2007, 119, 8170–8173.
12. K. A. Kuttiyiel, K. Sasaki, Y. Choi, D. Su, P. Liu and R. R. Adzic, *Energy Environ. Sci.*, 2012, 5, 5297.

13. H. Xu, Q. Fu, Y. Yao and X. Bao, *Energy Environ. Sci.*, 2012, 5, 6313.

14. M. Oezaslan, F. Hasche and P. Strasser, *J. Electrochem. Soc.*, 2012, 159 B444-B454.

15. M. Winter and R. J. Brodd, *Chem. Rev.*, 2004, 104, 4245-4269.

16. W. Vielstich, A. Lamm and H. A. Gasteiger, *Handbook of fuel cells fundamentals technology and applications*, John Wiley & Sons Ltd., London, 2003.

17. N. N. Kariuki, W. J. Khudhayer, T. Karabacak and D. J. Myers, *Acs Catal*, 2013, 3, 3123-3132.

18. L. Tang, B. Han, K. Persson, C. Friesen, T. He, K. Sieradzki and G. Ceder, *J. AM. CHEM. SOC.*, 2009, 132, 596-600.

19. Y. Shao-Horn, W. C. Sheng, S. Chen, P. J. Ferreira, E. F. Holby and D. Morgan, *Top. Catal.*, 2007, 46, 285-305.

20. Y. Shao, G. Yin and Y. Gao, *J. Power Sources*, 2007, 171, 558-566.

21. D. Higgins, M. A. Hoque, M. H. Seo, R. Wang, F. Hassan, J.-Y. Choi, M. Pritzker, A. Yu, J. Zhang and Z. Chen, *Adv. Funct. Mater.*, 2014, 24, 4325–4336.

22. M. H. Seo, S. M. Choi, E. J. Lim, I. H. Kwon, J. K. Seo, S. H. Noh, W. B. Kim and B. Han, *Chemsuschem*, 2014, DOI: 10.1002/cssc.201402258, in press.

23. R. Bashyam and P. Zelenay, *Nature*, 2006, 443, 63–66.

24. L. Qu, Y. Liu, J.-B. Baek and L. Dai, *ACS Nano*, 2010, 4, 1321-1326.

25. D. Deng, X. Pan, L. Yu, Y. Cui, Y. Jiang, J. Qi, W.-X. Li, Q. Fu, X. Ma, Q. Xue, G. Sun and X. Bao, *Chem. Mater.*, 2011, 23, 1188-1193.

26. Z. Chen, D. Higgins, A. Yu, L. Zhang and J. Zhang, *Energy Environ. Sci.*, 2011, 4, 3167.

27. H. Chung, C. Johnson, K. Artyushkova, M. Ferrandon, D. Myers and P. Zelenay, *Electrochem. Commun.*, 2010, 12, 1792-1795.

28. E. Proietti, F. Jaouen, M. Lefevre, N. Larouche, J. Tian, J. Herranz and J. P. Dodelet, *Nat. Commun.*, 2011, 2.

29. W. M. Li, J. Wu, D. C. Higgins, J. Y. Choi and Z. W. Chen, *Acs Catal*, 2012, 2, 2761-2768.

30. F. Jaouen, E. Proietti, M. Lefevre, R. Chenitz, J.-P. Dodelet, G. Wu, H. T. Chung, C. M. Johnston and P. Zelenay, *Energy Environ. Sci.*, 2011, 4, 114.

31. G. Wu, K. L. More, C. M. Johnston and P. Zelenay, *Science*, 2011, 332, 443-447.

32. M. Lefevre, E. Proietti, F. Jaouen and J. P. Dodelet, *Science*, 2009, 324, 71-74.

33. W. Li, A. Yu, D. C. Higgins, B. G. Llanos and Z. Chen, *J. Am. Chem. Soc.*, 2010, 132, 17056–17058.

34. N. Ramaswamy, U. Tylus, Q. Jia and S. Mukerjee, *J. Am. Chem. Soc.*, 2013, 135, 15443−15449.

35. Y. Bing, H. Liu, L. Zhang, D. Ghosh and J. Zhang, *Chem. Soc. Rev.*, 2010, 39, 2184-2202.

36. R. R. Adzic, J. Zhang, K. Sasaki, M. B. Vukmirovic, M. Shao, J. Wang, A. U. Nilekar, M. Mavrikakis, J. Valerio and F. Uribe, *Top. Catal.*, 2007, 46, 249-262.

37. P. Mani, R. Srivastava and P. Strasser, *J. Power Sources*, 2011, 196, 666-673.

38. B. Hammer and J. K. Norskov, *Nature*, 1995, 376, 238–240

39. J. Greeley, I. E. L. Stephens, A. S. Bondarenko, T. P. Johansson, H. A. Hansen, T. F. Jaramillo, J. Rossmeisl, I. Chorkendorff and J. K. Nørskov, *Nature Chem.*, 2009, 1, 552–556.

40. M. Shao, K. Sasaki, N. S. Marinkovic, L. Zhang and R. R. Adzic, *Electrochem. Commun.*, 2007, 9, 2848–2853.

41. M. H. Shao, P. Liu, J. Zhang and R. R. Adzic, *J. Phys. Chem. B*, 2007, 111, 6772-6775.

42. H. M. P. K. Shen, *Electrochem. Commun.*, 2006, 8, 588-594.

43. M.-S. Liao and S. Scheinera, *J. Chem. Phys.*, 2002, 117, 205.

44. P. Hohenberg and W. Kohn, *Phys. Rev.*, 1964, 136, B864–B871.

45. W. Kohn and L. J. Sham, *Phys. Rev. A*, 1965, 140, 1133–A1138.

46. G. Kresse and J. Furthmüller, *Phys. Rev. B*, 1996, 54, 11169.

47. J. P. Perdew, K. Burke and M. Ernzerhof, *Phys. Rev. Lett.*, 1996, 77, 3865.

48. G. Kresse and J. Furthmuller, *Comput. Mater. Sci.*, 1996, 6, 15.

49. G. Kresse and D. Joubert, *Phys. Rev. B*, 1999, 59, 1758

50. P. E. Blöchl, *Phys. Rev. B*, 1994, 50, 17953.

51. M. Methfessel and A. T. Paxton, *Phys. Rev. B*, 1989, 40, 3616-3621.

52. K. M. Ho, C. L. Fu, B. N. Harmon, W. Weber and D. R. Hamann, *Phys. Rev. Lett.*, 1982, 49, 673-676.

53. S. Baranton, C. Coutanceau, C. Roux, F. Hahn and J. M. Leger, *J. Electroanal. Chem*, 2005, 577, 223-234.

54. D. R. Lide, *CRC handbook of chemistry and physics (86th edition)*, 2005.

55. B. I. Lundqvist, O. Gunnarsson, H. Hjelmberg and J. K. Norskov, *Surf. Sci.*, 1979, 89, 196-225.

56. B. Hammer and J. K. Nørskov, *Advance in Catalysis*, 2000, 45, 71-129.

57. J. E. Huheey, E. A. Keiter and R. L. Keiter, *Inorganic Chemistry: Principles of Structure and Reactivity*, Prentice Hall, 1997.

58. H. Nakashima, J. Y. Hasegawa and H. Nakatsuji, *J. Comput. Chem.*, 2006, 27, 426-433.

59. A. R. Albuquerque, J. Maul, E. Longo, I. M. G. d. Santos and a. J. R. Sambrano, *J. Phys. Chem. C*, 2013, 117, 7050−7061.

60. J. Zagal, P. Bindra and E. Yeager, *J. Electrochem. Soc.*, 1980, 127, 1506-1517.

61. J. Zagal, M. Paez, A. A. Tanaka, J. R. Dossantos and C. A. Linkous, *J. Electroanal. Chem.*, 1992, 339, 13-30.

62. N. Ramaswamy and S. Mukerjee, *Adv. Phys. Chem.*, 2012, 2012 17.

63. M. H. Seo, S. M. Choi, H. J. Kim and W. B. Kim, *Electrochem. Commun.*, 2011, 13 182–185.

64. J. Guo, A. Hsu, D. Chu and R. Chen, *J. Phys. Chem. C* 2010, 114, 4324–4330.

65. N. M. Markovic, B. N. Grgur and P. N. Ross, *J. Phys. Chem. B*, 1997, 101, 5405-5413.

66. U. A. Paulus, T. J. Schmidt, H. A. Gasteiger and R. J. Behm, *J. Electroanal. Chem.*, 2001, 495 134–145.

67. K. J. J. Mayrhofer, D. Strmcnik, B. B. Blizanac, V. Stamenkovic, M. Arenz and N. M. Markovic, *Electrochim. Acta*, 2008, 53 3181–3188.

68. H. Kim, K. Lee, S. I. Woo and Y. Jung, *Phys. Chem. Chem. Phys.*, 2011, 13, 17505–17510.

69. H. Tominaga, W. Ikeda and M. Nagai, *Phys. Chem. Chem. Phys.*, 2011, 13, 2659–2662.

70. J. K. Nørskov, J. Rossmeisl, A. Logadottir, L. Lindqvist, J. R. Kitchin, T. Bligaard and H. Jo´nsson, *J. Phys. Chem. B*, 2004, 108, 17886-17892.

71. S. F. Huang, K. Terakura, T. Ozaki, T. Ikeda, M. Boero, M. Oshima, J. Ozaki and S. Miyata, *Physical Review B*, 2009, 80.

72. B. Han, V. Viswanathan and H. Pitsch, *J. Phys. Chem. C*, 2012, 116, 6174−6183.

73. S. H. Noh, D. H. Kwak, M. H. Seo, T. Ohsaka and B. Han, *Electrochimica Acta* 2014, DOI: 10.1016/j.electacta.2014.03.076.

74. P. Atkins and J. D. Paula, *Physical Chemistry, eight ed.*, Oxford University Press, Oxford, UK, 2006.

75. J. K. Seo, A. Khetan, M. H. Seo, H. Kim and B. Han, *J. Power Sources*, 2013, 238 137-143.

76. S. H. Noh, M. H. Seo, J. K. Seo, P. Fischer and B. Han, *Nanoscale*, 2013, 5, 8625-8633.

77. L. Tang, B. Han, K. Persson, C. Friesen, T. He, K. Sieradzki and G. Ceder, *J. Am. Chem. Soc.*, 2010, 132, 596–600.

78. W. H. Qi and M. P. Wang, *J. Mater. Sci. Lett.* , 2002, 21, 1743-1745.

79. I. C. Stefan, Y. B. Mo, S. Y. Ha, S. Kim and D. A. Scherson, *Inorg. Chem.*, 2003, 42, 4316-4321.

Table 1. Bond lengths between the Fe and N atoms, O and O_2 adsorption energies, and cohesive energies of Fe and FeO in the investigated Fe-Pc and Fe-SPc structures.

	Fe-N1 Å	**Fe-N2** Å	**Fe-N3** Å	**Fe-N4** Å	$E_{ads\text{-}O}$ eV	$E_{ads\text{-}O2}$ eV	$E_{coh\text{-}Fe}$ eV	$E_{coh\text{-}FeO}$ eV
Fe-Pc	1.934	1.934	1.934	1.938	-4.02	-0.92	9.80	10.15
Fe-SPc	1.938	1.941	1.925	1.924	-4.37	-0.98	9.53	10.22

Figures

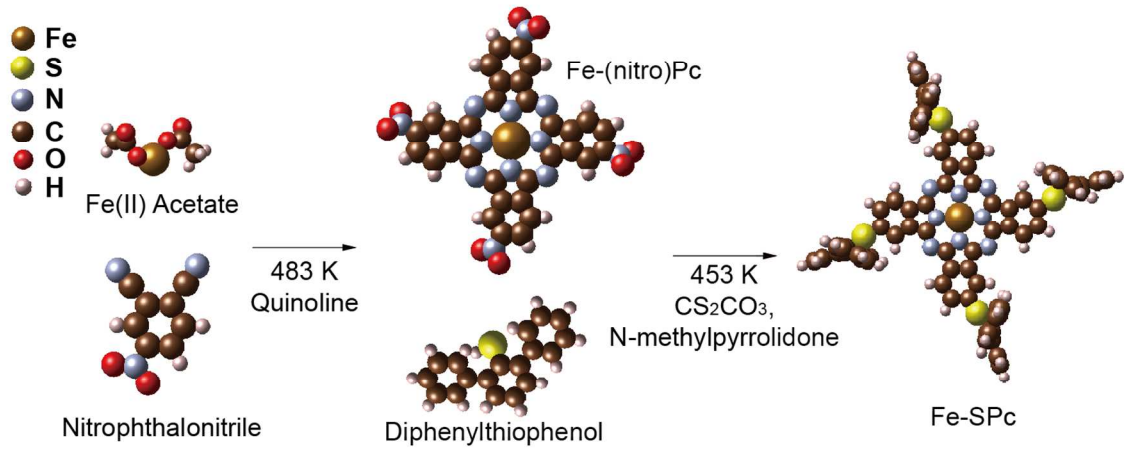

Fig. 1. Schematic illustration of the synthesis of Fe-SPc.

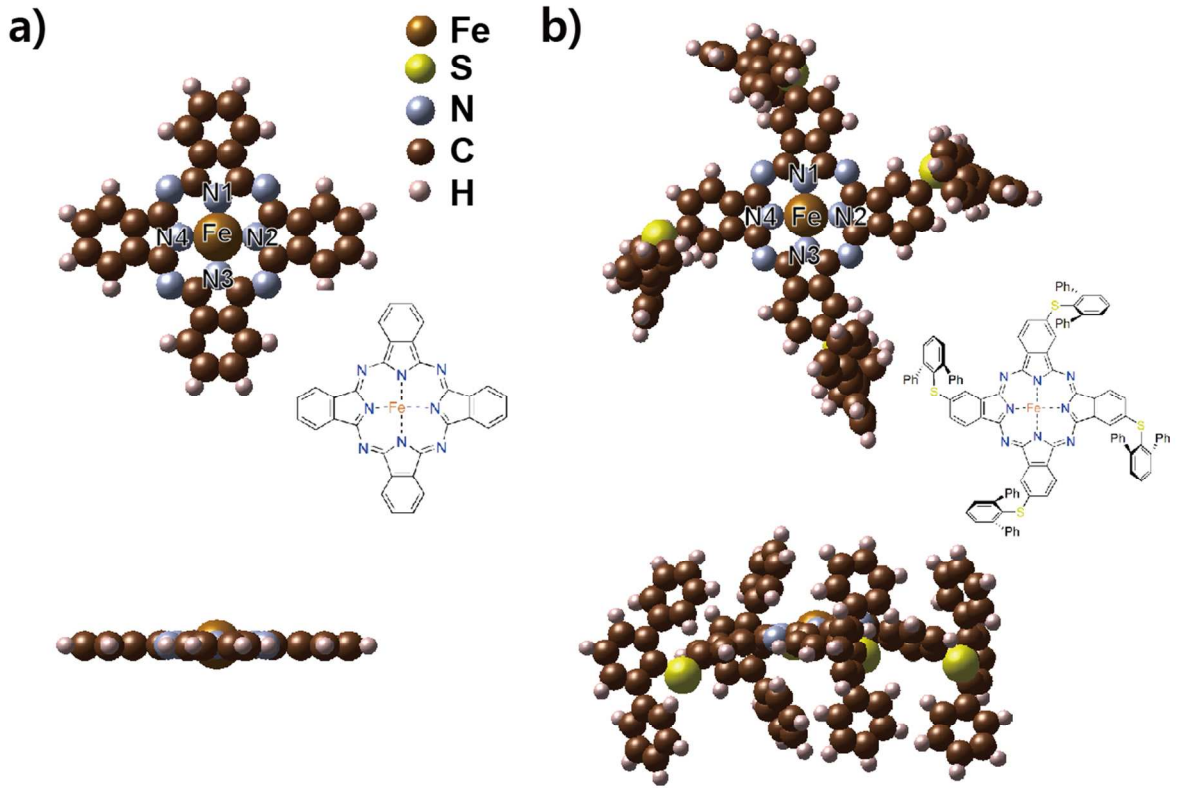

Fig. 2. Top and side views of the model structures for (a) Fe-Pc and (b) Fe-SPc.

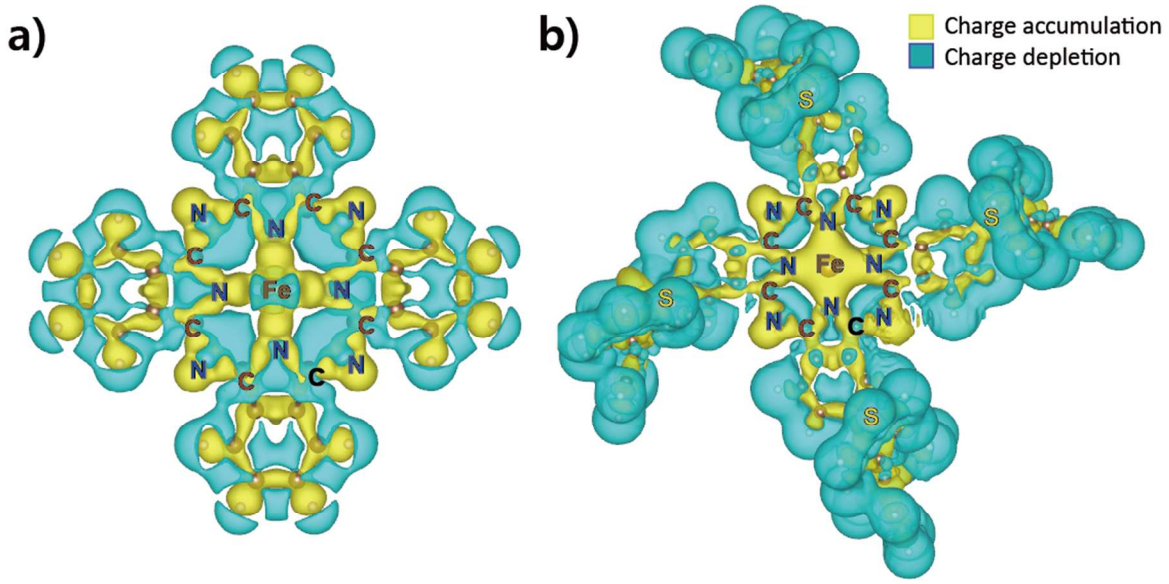

Fig. 3. Charge density changes of Fe-Pc and Fe-SPc

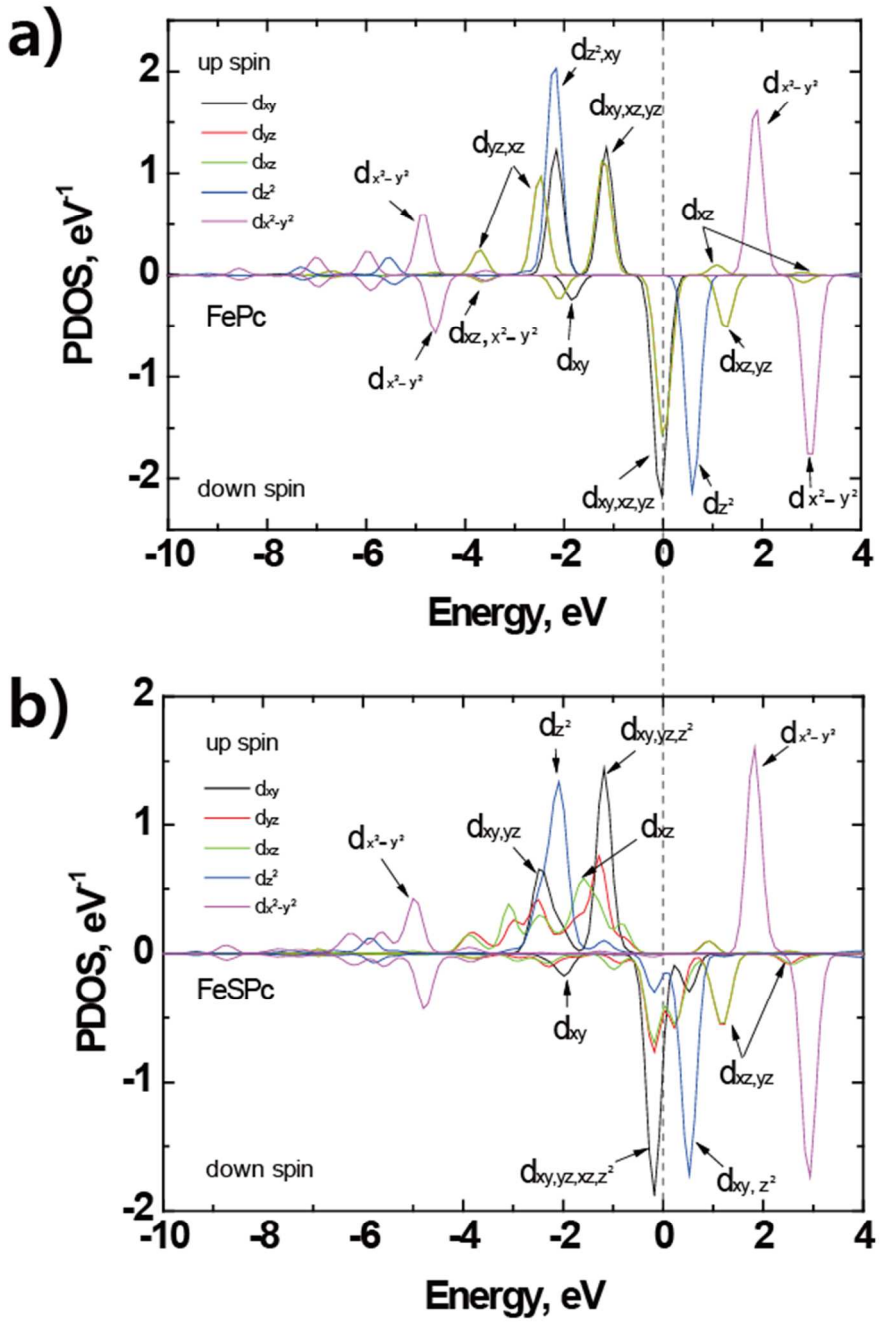

Fig. 4. PDOS for (a) Fe-Pc and (b) Fe-SPc calculated with the d_{xy}, d_{xz}, d_{yz}, d_{x2-y2} and d_{z2} orbitals by DFT methods. All of the densities of states are shifted so that the Fermi energy is zero.

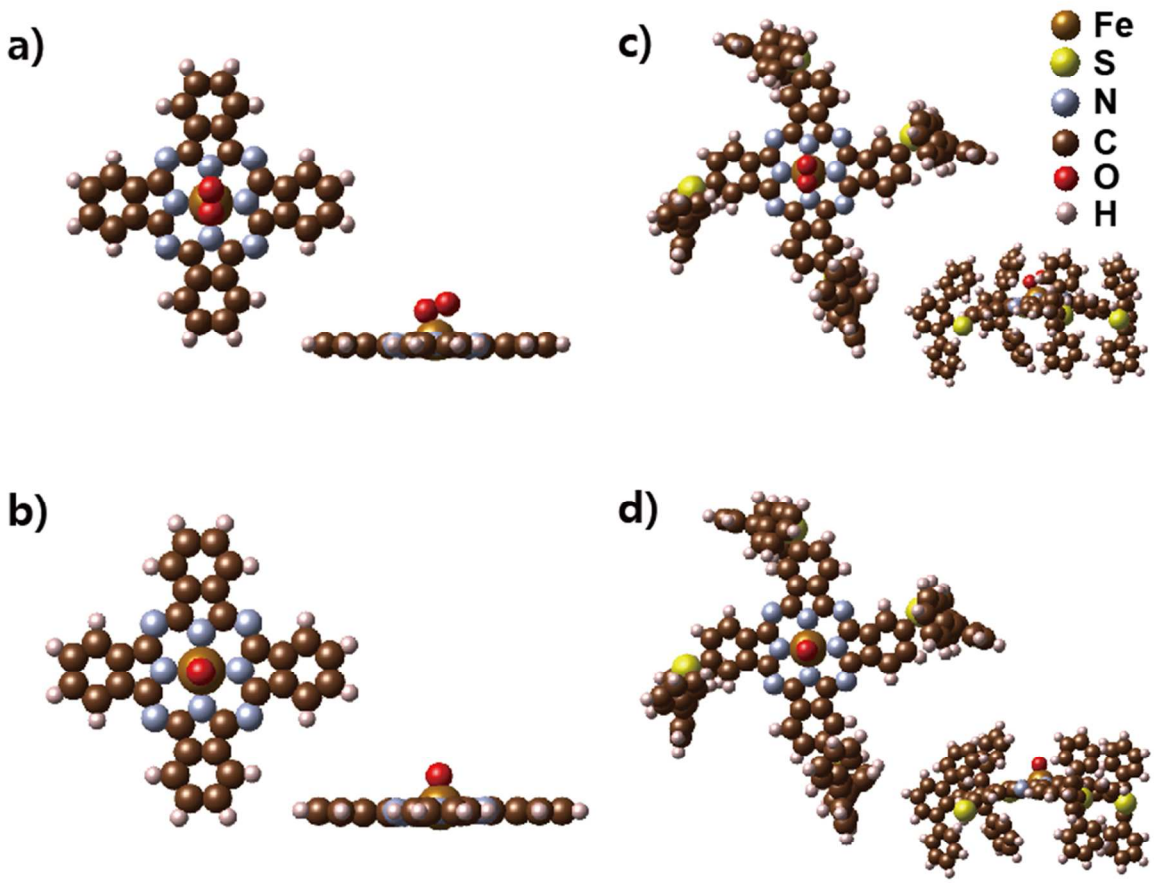

Fig. 5. Top and side views of the model structures for O_2 and O adsorbed (a, b) Fe-Pc and (c, d) Fe-SPc.

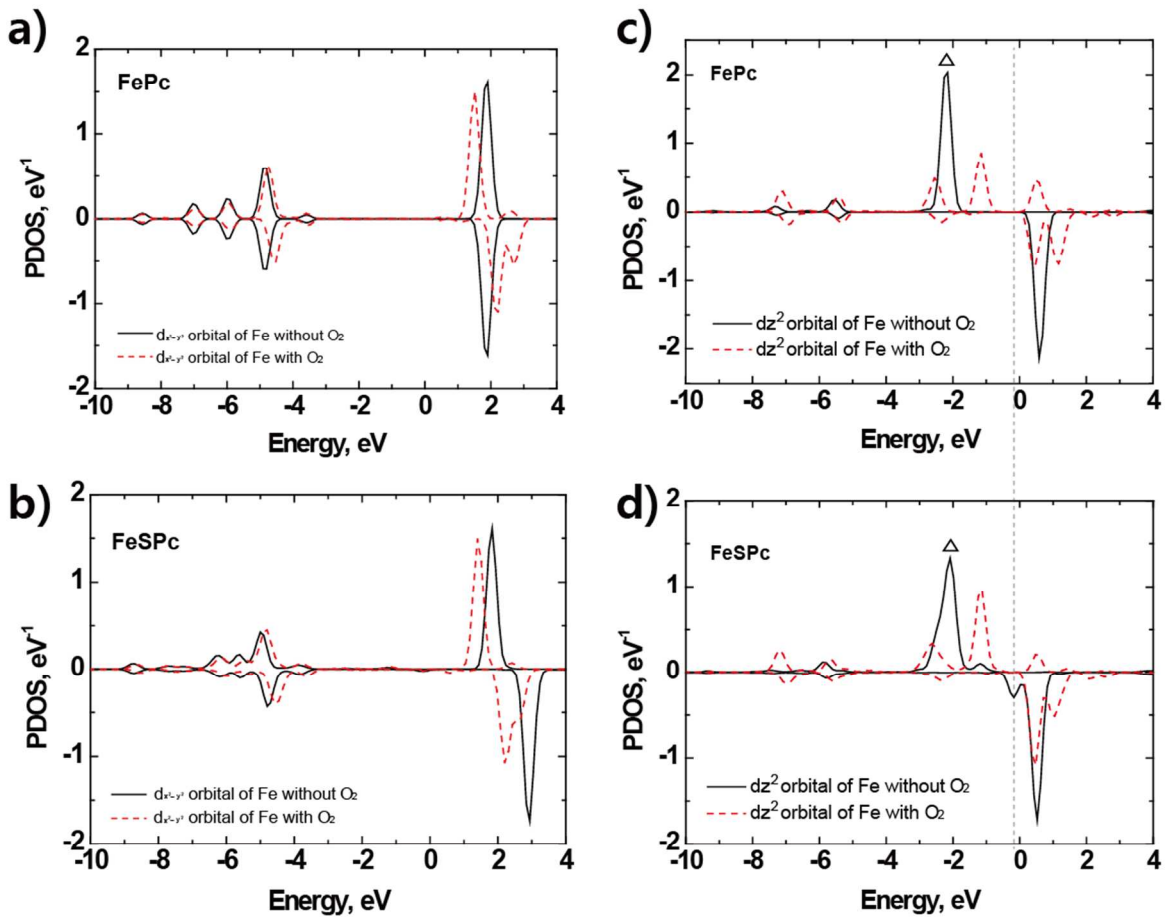

Fig. 6. PDOS of (a, b) d_{x2-y2} and (c, d) d_{z2} orbitals in (a) Fe-Pc and (b) Fe-SPc before/after adsorption of O_2 calculated by DFT methods. All of the densities of states are shifted so that the Fermi energy is zero.

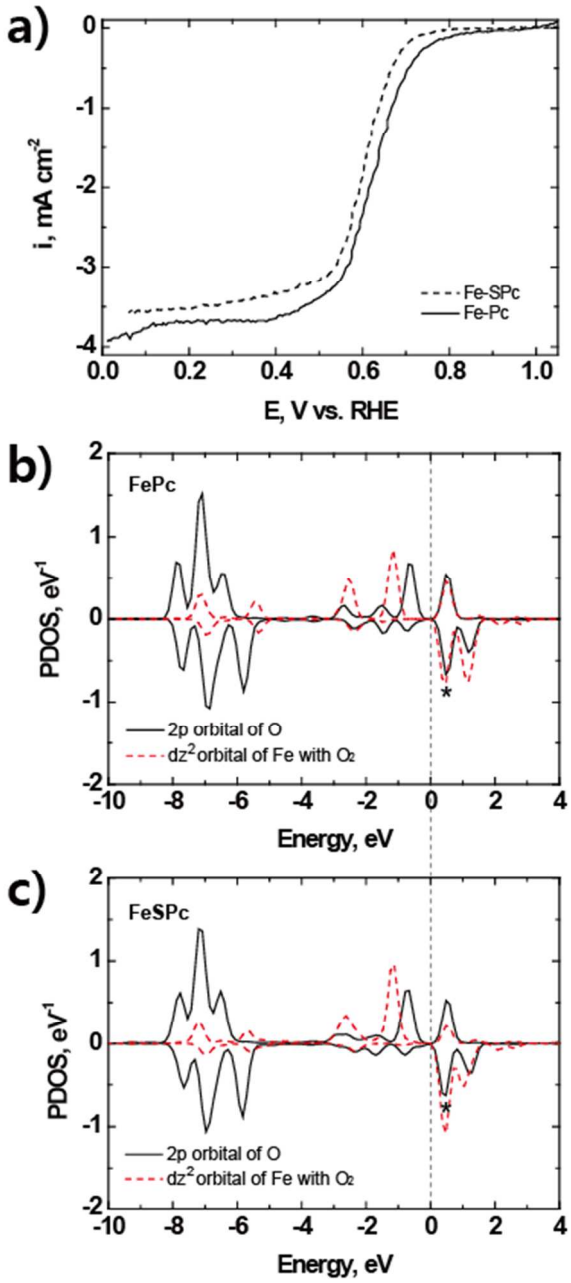

Fig. 7. (a) Polarization curves on Fe-Pc/KJ300 (straight line) and Fe-SPc/KJ300 (dashed line) for the ORR in O_2 saturated 0.1 M $HClO_4$. PDOS of O_2 2p and Fe d_{z2} orbitals in O_2 adsorbed (b) FePc and (c) Fe-SPc calculated by DFT methods. All of the densities of states are shifted so that the Fermi energy is zero. Experimental data of Fig (a) is reproduced from [23], copyright 2010, with permission of The American Chemical Society

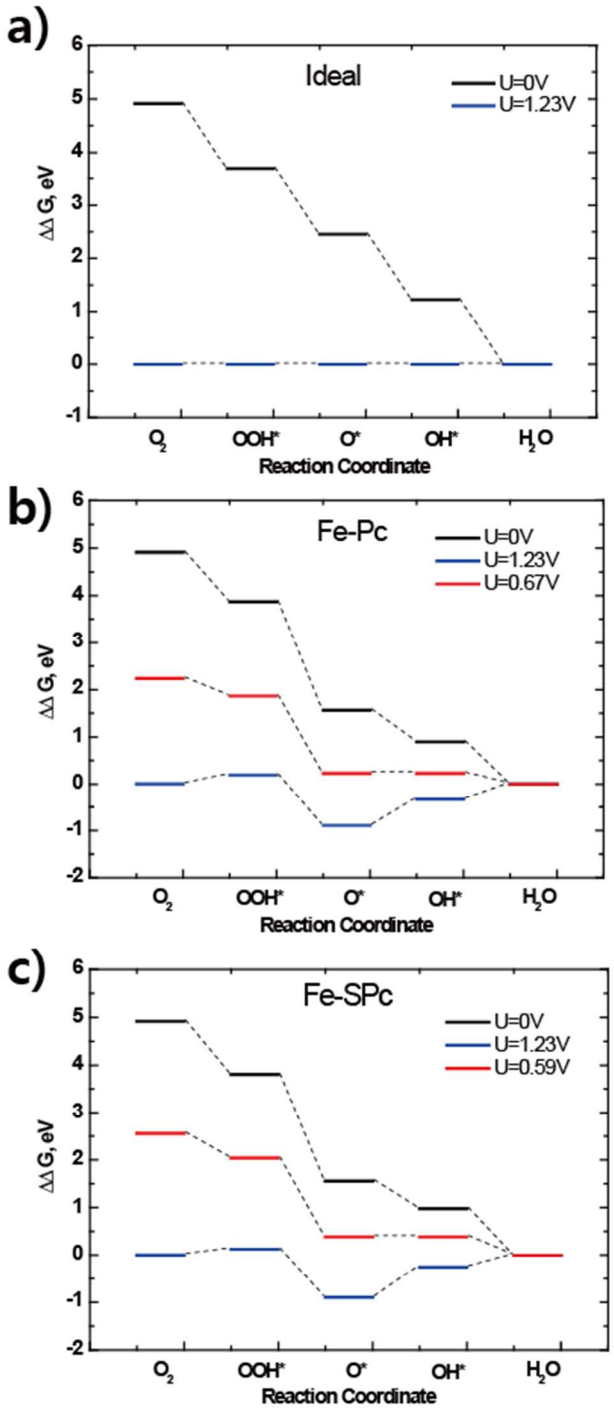

Fig.8. Standard free energy diagram of (a) ideal, (b) Fe-Pc and (c) Fe-SPc for ORR at zero potential (U=0), equilibrium potential for ORR (U=1.23 V) and at the potential for which all steps become energetically negative at pH=0 and T=298 K.

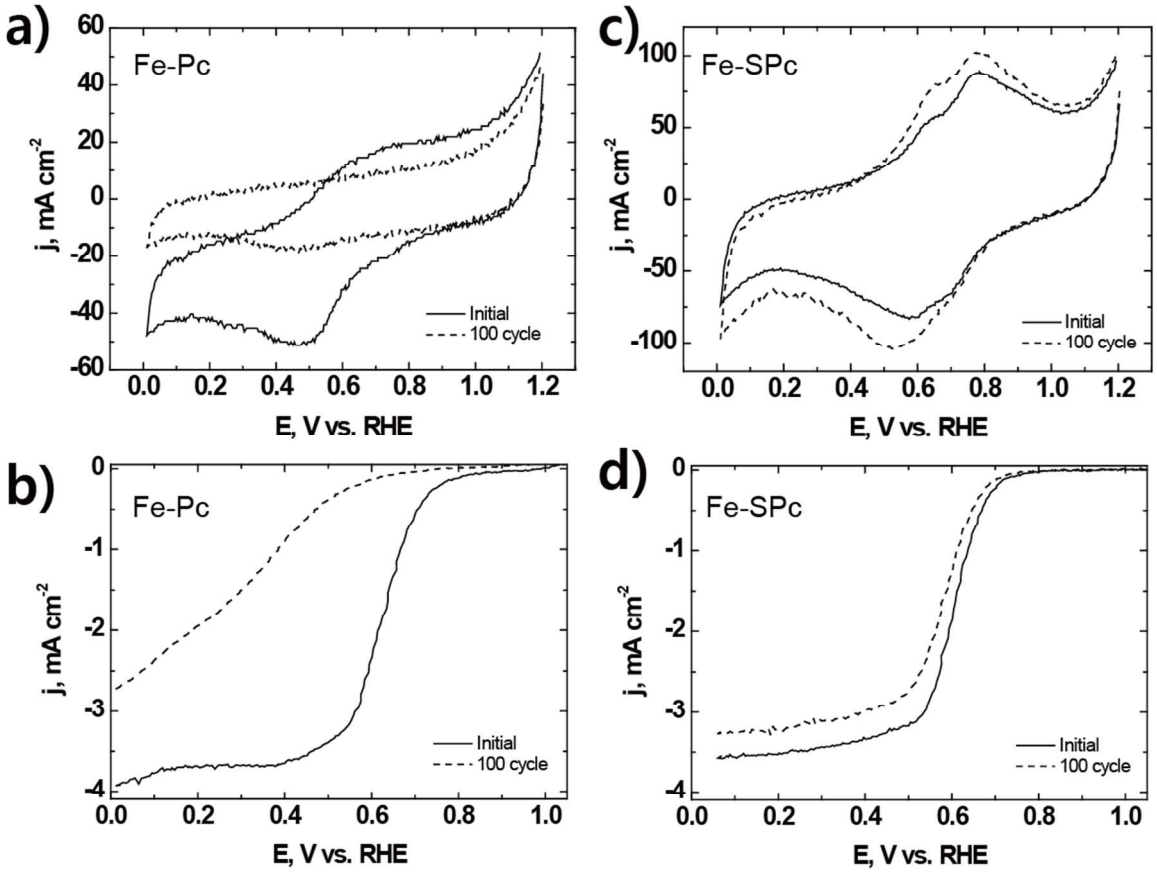

Fig. 9. (a, c) Cyclic voltammograms and (b, d) ORR polarization curves on Fe-Pc/KJ300 and Fe-SPc/KJ300 before and after 100 potential cycles in O_2 saturated 0.1 M $HClO_4$. This data is reproduced from [23], copyright 2010, with permission of The American Chemical Society.